CO_2-BRINE DISPLACEMENT IN HETEROGENEOUS CARBONATES

H. Ott*, C.H. Pentland, and S. Oedai
Shell Global Solutions International B.V., 2288 GS Rijswijk, The Netherlands.

This paper was prepared for presentation at the International Symposium of the Society of Core Analysts held in Avignon, France, 8–11 September, 2014

ABSTRACT

The investigation of CO_2-brine displacement in porous rock is important to predict plume migration and initial pore-space utilization in CO_2 storage. The measurement of relative permeability saturation functions ($k_r(S_w)$) characterizing displacement requires relatively homogeneous core material. Carbonates, however, are often heterogeneous on various length scales. While microscopic heterogeneity determines $k_r(S_w)$, larger-scale heterogeneity that is not statistically represented in the measured volume affects the investigation. In this paper we present CO_2-brine unsteady-state core flood experiments in order to characterize CO_2-brine primary drainage in Estaillades limestone. We describe the experiments by means of numerical simulations assuming 1-D homogeneous rock and parameterized $k_r(S_w)$ relationships. Assisted history matching methodologies were used to find the $k_r(S_w)$ parameters which minimize a mismatch function, giving the best match to the experimental data. The effects of larger-scale heterogeneity are still not taken explicitly into account (just by sample selection) and are a subject for further discussion.

INTRODUCTION

CO_2-plume migration in deep saline aquifers and the initial utilization of the pore space for CO_2 storage is to a large extent subject to CO_2-brine immiscible displacement as determined by relative permeability ($k_r(S_W)$) and capillary pressure ($p_C(S_W)$) saturation functions. These functions describe the microscopic displacement efficiency as well as the macroscopic bypassing by channeling and/or viscous fingering. Hence the characterization of the primary drainage process is essential for predicting the plume migration and the efficiency of storage.

CO_2-brine displacement in relatively homogeneous sandstone has recently been investigated by e.g. Ott and Berg (Ott et al., 2011; Berg et al., 2013) and Akbarabadi and Piri, 2013, and with sub-core heterogeneity by Perrin and Benson, 2010. Despite the difficulties that CO_2-brine displacement implies—i.e. high viscosity ratio, low displacement efficiency, chemical reactivity—public data on well sorted sandstone are more or less in agreement and can be described by a minimum set of parameters (usually the Corey relative permeability model (Brooks and Corey, 1964) is used). The situation turns out to be more demanding for complex carbonates; carbonates are often heterogeneous on various length scales. While microscopic heterogeneity determines the shape of $k_r(S_w)$, larger-scale heterogeneity that is statistically not represented in the respective sample volume affects the investigation and makes the result scale-

dependent—i.e. dependent on the size of the sample—and dependent on the exact location of sampling.

In this paper we present our initial investigation into CO_2-brine primary drainage in Estaillades limestone. We performed CO_2-brine and decane-brine unsteady-state (USS) and steady-state (SS) experiments. We history match core flood data, taking different relative permeability parameterizations, with varying degrees of complexity, into account in a one-dimensional simulation model. Macroscopic heterogeneity is not explicitly taken into account, but we briefly describe sample heterogeneity on the core scale and the core to core variation to open a discussion on how to deal with heterogeneity in CO_2-brine displacement and how to reliably and practically derive meaningful parameters for field-scale simulations.

EXPERIMENTS & RESULTS

The experiments were performed on Estaillades limestone with a pure calcite mineralogy. The pore structure is bi-modal, as indicated in the µCT cross-section, the MICP curve and the respective pore throat distribution shown in Figure 1. The average porosity is ~0.3 and the average permeability is ~220 mD with a sample to sample variation of ~20%. The sample dimensions were 3 inches in diameter and 15 cm in length.

The cores were initially saturated with brine, which was then displaced by the non-wetting phase. Two experiments were performed: the actual CO_2-brine primary drainage experiment, and, on the same rock samples, experiments using decane as the displacing phase, which allows comparison with standard SCAL experiments. From these core floods primary drainage relative permeability can be inferred.

As can be seen from Figure 2, the rock type is not only heterogeneous at the pore scale (see Figure 1), but also at a scale that is not statistically represented in the—relatively large—sample volume. Figure 2 shows the porosity profile of three samples studied in this work. The lower rows show the CO_2 saturation profile under flow conditions at the end of the CO_2-brine primary drainage experiments as 1-D and 3-D saturation profiles. The porosity profiles were derived from CT scans. The samples show different degrees of porosity heterogeneity; while the left sample is relatively homogeneous, it has a general porosity variation of about 0.05 in porosity units. It is interesting that there is no obvious correlation between the porosity profiles and the CO_2 saturation profiles at the end of the respective CO_2 flood (taking the capillary end-effect into account) as it has been reported on sandstone by Perrin and Benson, 2010. In conclusion, we found that the porosity profiles and also the single phase tracer floods (not shown here—see e.g. Ott et al. 2013) do not relate to the performance (efficiency) of two-phase displacement. This means that whether or not a sample can be considered as homogeneous can only be decided after the experiment.

All USS experiments were performed at a pressure of 100 bar and a temperature of 50°C, corresponding to an aquifer depth of about 1000 m. The experimental setup and the procedures we follow in this study have been reported by Berg and Ott (Berg et al., 2013; Ott et al., 2013). In brief: the core was pre-saturated with (CsCl doped) brine (S_W=1) that was equilibrated at experimental conditions with CO_2 and the mineral phase of the rock.

In subsequent experiments, water-saturated CO_2 and decane were injected at rates of 0.44 ml/min and 0.25 ml/min, respectively immiscibly displacing the brine phase. During displacement we measured the pressure drop, ΔP, and the 3-D CT (computer tomography) density profiles a as function of time, reflecting the fluid saturation change. The cumulative brine production is additionally and independently measured.
Data of a CO_2-brine (lower row) and a decane-brine (upper row) core flood are shown in Figure 3. Both experiments were subsequently performed on the same rock sample under the same conditions with a cleaning step inbetween (see Berg et al., 2013). We focused on the third sample in Figure 2, which is considered as homogeneous. Figure 3 shows ΔP (left), the brine-production curve (middle), and the CO_2 saturation profiles at three different time steps (right) during the experiment. The data show the quantitative difference between decane-brine and CO_2-brine displacement, reflecting the differences in fluid viscosity, interfacial tension (IFT), and relative fluid permeability, $k_r(S_W)$. While viscosities and IFT are known, we extract $k_r(S_W)$ by means of numerical simulations, which is the subject of the following chapters.

DATA INTERPRETATION

We interpreted our experimental data with the aid of coreflood simulations. Coreflood simulations have traditionally involved a manual tuning of parameters in order to achieve a match to the observed experimental data. More recently tools have emerged that partially automate this process: so-called assisted history matching tools. More commonly used in field-scale reservoir simulation (e.g. Oliver and Chen, 2011; Oliver et al., 2008; Rwechungura et al., 2011), such approaches have also been applied to coreflood simulation (Kerig and Watson, 1987; Loeve et al., 2011; Okabe, 2005; Wang and Buckley, 2006).
We used a Shell proprietary stochastic uncertainty management tool and reservoir simulator (Por et al., 1989) to interpret our experimental dataset. Here we describe the methodology used and present the results of the matching exercise.

Coreflood Model & Measured Data

1-D horizontal models of the core, discretized into 31 grid cells (2 for the inlet/outlet and 29 for the core) were used. To aid numerical stability and to better resolve inlet and outlet effects, the first (and last) four core cells were 0.1, 0.2, 0.4, and 0.8 times the length of the central cell, with the smallest cells being located at the ends of the core. The inlet and outlet cells were 0.001 times the length of the central core cell. Constant values of porosity (0.297) and permeability (260 mD) were assigned to all core cells. The inlet and outlet cells contained injection and production wells respectively. The injection well operated at a constant injection flow rate, while the production well operated at a constant pressure constraint, replicating the experimental conditions. For the decane-brine simulations a simple black-oil PVT description was used and for the CO_2-brine simulations a Cubic plus Association Equation of State was used to model partitioning of the CO_2 and H_2O between the supercritical CO_2 phase and the aqueous phase. To rule out uncertainties regarding the saturation state of the injected CO_2, we modelled both dry and

pre-equilibrated CO_2 injections. The best agreement was found with the equilibrated phase simulations; only these results will be shown and discussed here.
Capillary forces were accounted for, with the capillary pressure curve being scaled from mercury-air data, accounting for changes in interfacial tension. The objective was to determine the relative permeabilities and as such these were parameterized and varied as described below.
From the measured water production and differential pressure data we selected a limited number of points to act as the observed data in the assisted history matching exercise (herein referred to as observables), thus simplifying the matching process. Two data points were selected from both the water production and differential pressure dataset. These points were chosen so that the late time and breakthrough behaviors were captured (Table 1). By selecting two points each from the production and pressure data these data sources carry equal weighting (note it is possible for the user to define a weighting per observable, all weights were set to unity). The standard deviations were based on pump and gauge accuracy.

Assisted History Matching Methodology
The assisted history matching approach consists of four main elements: a parameterization of the functions of interest (in this case relative permeability); a sampling of the parameter space using experimental design methods; the creation and quality control of a proxy model; and the subsequent interrogation of the proxy model to identify best matches to the observed experimental data.

1. Relative Permeability Parameterization
Assisted history matching works by varying input parameters in order to achieve a match between simulated and observed data. In the case of our coreflood experiment it is the relationship between relative permeability and saturation, which is unknown and which must be varied in order to get an acceptable match. To simplify this process three parameterized functions were investigated (Brooks and Corey, 1964; Lomeland et al., 2005; Masalmeh et al., 2007), as summarized in Table 2. Working with parameterized functions can limit the number of simulations necessary to build a good quality proxy model. However, the disadvantage is that the shapes of the resulting relative permeability curves are constrained by the functional form of the equations.
Each variable parameter was assigned a range and a probability distribution. We used uniform distributions for all parameters. The minimum and maximum values of the parameters are summarized in Table 3. These ranges were assigned based on an understanding of typical relative permeability behavior, or in the case of the empirical matching parameters of Lomeland et al. (2005) on the guidance given in the original publication. Typically these ranges were wide enough to allow a satisfactory match to be achieved, however, in the case of the wetting phase Corey exponents our initial ranges proved inadequate and a match was not achieved. We had to subsequently re-visit our initial range and expand it. This explains the high maximum wetting phase Corey exponents used (Table 3). As we will discuss later, the sharp fall-off in wetting phase

relative permeability—which required these high Corey exponents—is a characteristic of the system investigated.

2. Experimental Design

With the parameters and their ranges stipulated, it is possible to explore the resulting parameter space by running coreflood simulations with different combinations of parameter values. To do this efficiently, experimental design methods were used. We first ran a tornado design, where parameters were systematically varied one at a time to either their minimum or maximum values, while keeping the remaining parameters at their base values. The resulting tornado plots (not shown) were used to understand which parameters are well constrained by the measured data. We then ran a Box-Behnken design (Box and Behnken, 1960) in addition to a space-filling and a latin-hypercube (McKay et al., 1979) design. The Box-Bhenken and space-filling designs were used to construct our proxy model (see below), while the latin-hypercube design was used to subsequently test the quality of the proxy model.

3. The Proxy Model

Our observables were selected from the measured water production and pressure difference experimental measurements. Based on the outputs of the simulations (generated for parameter values coming from experimental design), a proxy model was generated for each of the observable points in Table 1. The proxy is described by a second order polynomial which is a function of the unknown parameters. The advantage of the proxy model is that it allows a computationally cheap evaluation (estimation) of the simulated observable, and hence a faster history matching process. Our proxy models were generated based on the results of the Box-Behnken and space-filling design. We subsequently checked the quality of the model by comparing it against the results of the latin-hypercube design, our quality criteria being that the simulated observable values should be within ± 10% of the value approximated by the proxy.

4. Best Match Identification

Having created and checked our proxy model, we then interrogated it in order to find the best matches to our measurements. This was done by minimizing the mismatch function:

$$V = \sum_{i=1}^{N_{obs}} w_i (d_i - y_i)^2, \quad (1)$$

where V is the mismatch function, w_i the weight, d_i the observed data, and y_i the simulated value. First we sampled the proxy surfaces one thousand times with a Monte Carlo approach, the best four matches from which were added to our proxy, which was then recomputed. We then sampled a further one thousand times with a Markov chain Monte Carlo approach (Andrieu et al., 2003). Based on this sampling, the parameter values for the four best match cases were simulated in our simulation model to confirm the quality of these best match cases.

Best Match Cases

Table 4 summarizes the best match cases identified from the workflow described above, while Figure 3 compares the simulated water production, pressure drop, and saturation profile responses to the measured data. The best match to the decane-brine dataset was achieved with the LET and Modified Corey parameterizations and the best match to the CO_2-brine dataset was achieved with the Modified Corey parameterization. Table 5 summarizes the parameter values for the best match cases and Figure 4 shows the best match relative permeability curves.

DISCUSSION & CONCLUSION

We performed experiments on three different samples of the same rock type, from which we have chosen the most homogeneous one for further investigation using numerical modeling. The selection has been done in order to describe the core flood in a homogeneous model by the smallest possible number of parameters. The selection circumvents the explicit description of core-scale heterogeneity that would effectively lead to a downscaling of the problem, raising questions about general validity and practical use. The heterogeneity has been defined on the basis of the final CO_2 saturation profile rather than on porosity data only, as discussed in context of Figures 1 and 2.

The presented unsteady state experiments provide valuable insight in the fundamental CO_2-brine displacement and are close to the actual field displacement process. However, the determination of relative permeability is non-trivial. The typically sharp transition during primary drainage from brine production before breakthrough to predominantly CO_2 or decane production provides a limited dataset to which simulation models can be constrained. Furthermore, the limited accessible saturation range, in our case $0.6 < S_w < 1.0$, is investigated due to the competition between viscous and capillary forces: the application of a viscous pressure drop across the core displaces a certain amount of water before the remainder is held in place by capillary forces. Note that this is not the irreducible water saturation (cf. non-zero relative permeability end-points in Figure 4). If we were to increase the viscous pressure drop (by increasing the injection flow rate), more water would be displaced. As a result of these limitations our interpretation is that the non-wetting phase only invaded the larger pores in this dual porosity carbonate rock; the sub-micron pores were not invaded.

Additional information before and after breakthrough is obtained by in-situ saturation monitoring. The flood front propagation and the final saturation profile were used as independent benchmark for the simulations. The comparison of experimental results and simulations as shown in Figure 3 is reasonable considering the simplifications applied in the simulation model, especially at early and late time (first and last scan in the right panels).

The resulting relative permeability functions are shown in Figure 4. We plot the best fit of each of the applied parameterizations for comparison. The decane-brine results are shown in the left panels and the CO_2-brine results in the middle. The respective lower panel shows the same datasets on a logarithmic scale. The best fit of the decane-brine was obtained by LET parameterization and the CO_2-brine system was best described by the modified Corey description with the parameters provided in Table 5; both datasets are compared in the right panels. We observe that both the wetting and the non-wetting phase

relative permeability in the CO_2-brine system tend to be smaller than those in the decane-brine system at comparable water saturations. For the non-wetting phase, this is consistent with previous studies on Berea sandstone (Berg et al. 2013, and the references given in Benson et al., 2013). However for the wetting phase, a previous study showed the water relative permeability to be higher in the CO_2-brine system than in the decane-brine system (Berg et al. 2013), while a compilation of data from different studies with different sample preparation methods showed the opposite trend (Benson et al., 2013).

In the left panels of Figure 5, the results from the decane-brine USS experiment are compared to the results obtained from the standard steady-state approach (SS) in which decane and brine is injected simultaneously with flow rates adjusted during the experiments in order to reach steady-state conditions at different fractional flows. Two SS experiments were performed on two samples of smaller size. Both SS datasets show comparable brine K_r branches, but deviate in oil relative permeability. Using both SS datasets to describe the USS core flood failed. The obtained pressure drop and production curve are shown in the respective panels in Figure 3. The main difference between the SS and USS is the relatively sharp drop of the brine branch in USS compared to SS. Since we believe in the quality of the performed experiments, we raise the question about the comparability of SS and USS, especially in the case where capillary heterogeneity is a characteristic of displacement. While in SS the flow rate of the individual phases varies by one to two orders of magnitude during the experiment changing the capillary number respectively, the capillary number is constant in USS approach. In the present case, the USS flow rate (corresponding to a velocity of 1 ft/day) was in the same order as the lowest decane flow rate in SS—hence the choice of the method to determine relative permeability could be a concern.

Further work needs to be done to understand (1) whether or not the obtained relative permeability saturation function is representative for the rock type and if not (2) how to effectively include the core-scale (capillary) heterogeneity into the picture. (3) If we effectively downscale the system by including heterogeneities, how to upscale it again in order to derive a useful function? These are questions we would like to address to the core analysis community.

ACKNOWLEDGEMENTS

The authors would like to thank Fons Marcelis and Ab Coorn for sample preparation and Niels Brussee and Hilbert van der Linde for performing steady state experiments.

NOMENCLATURE

k_{rw} = wetting phase relative permeability; k_{rnw} = non-wetting phase relative permeability; S_w = wetting phase saturation; S_{wn} = normalized wetting phase saturation; S_{wc} = connate (irreducible) wetting phase saturation S_{nwr} = residual non-wetting phase saturation (after imbibition); n_w = wetting phase Corey exponent; n_{nw} = non-wetting phase Corey exponent; c_w = empirical fitting parameter used when modifying the Corey functions; k_{rnw}^{w} = non-wetting phase relative permeability at connate (irreducible) wetting phase; saturation (also known as the non-wetting phase end point relative permeability); L_w^{nw} =

empirical parameter of the LET model for the wetting phase; L_{nw}^{w} = empirical parameter of the LET model for the non-wetting phase; E_{w}^{nw} = empirical parameter of the LET model for the wetting phase; E_{nw}^{w} = empirical parameter of the LET model for the non-wetting phase; T_{w}^{nw} = empirical parameter of the LET model for the wetting phase; T_{nw}^{w} = empirical parameter of the LET model for the non-wetting phase.

REFERENCES

* Corresponding author; Holger Ott; holger.ott@shell.com, research@holger-ott.de.

Akbarabadi, M., Piri, M., 2013. Relative Permeability Hysteresis and Capillary Trapping Characteristics of Supercritical CO_2/Brine Systems: An Experimental Study at Reservoir Conditions. Advances in Water Resources 52, 190–206. doi:10.1016/j.advwatres.2012.06.014

Andrieu, C., Freitas, N. de, Doucet, A., Jordan, M.I., 2003. An Introduction to MCMC for Machine Learning 50, 5–43. doi:10.1023/A:1020281327116

Benson, S., Pini, R., Reynolds, C., Krevor, S., 2013. Relative Permeability Analysis to Describe Multi-phase Flow in CO_2 Storage Reservoirs (No. 2). Global CCS Institute.

Berg, S., Oedai, S., Ott, H., 2013. Displacement and mass transfer between saturated and unsaturated CO_2–brine systems in sandstone. International Journal of Greenhouse Gas Control 12, 478–492. doi:10.1016/j.ijggc.2011.04.005

Box, G.E.P., Behnken, D.W., 1960. Some New Three Level Designs for the Study of Quantitative Variables. Technometrics 2, 455. doi:10.2307/1266454

Brooks, R.H., Corey, A.T., 1964. Hydraulic Properties of Porous Media, Hydrology Papers. Civil Engineering Dept., Colorado State Univ., Fort Collins, CO.

Kerig, P.D., Watson, A.T., 1987. A New Algorithm for Estimating Relative Permeabilities From Displacement Experiments. SPE Reservoir Engineering 2. doi:10.2118/14476-PA

Loeve, D., Wilschut, F., Hanea, R.H., Mass, J.G., van Hoof, P.M.E., van den Hoek, P.J., Douma, S.G., Van Doren, J.F.M., 2011. Simultaneous Determination of Relative Permeability and Capillary Pressure Curves by Assisted History Matching Several SCAL Experiments. Presented at the International Symposium of the Society of Core Analysts, Austin, Texas, USA.

Lomeland, F., Ebeltoft, E., Thomas, W.H., 2005. A New Versatile Relative Permeability Correlation. Presented at the International Symposium of the Society of Core Analysts, Toronto, Canada.

Masalmeh, S., Abu-Shiekah, I., Jing, X., 2007. Improved Characterization and Modeling of Capillary Transition Zones in Carbonate Reservoirs. SPE Reservoir Evaluation & Engineering 10. doi:10.2118/109094-PA

McKay, M.D., Beckman, R.J., Conover, W.J., 1979. A Comparison of Three Methods for Selecting Values of Input Variables in the Analysis of Output from a Computer Code. Technometrics 21, 239. doi:10.2307/1268522

Okabe, H., 2005. Bridging Pore to Core-Scale Flow Properties Using Pore-Scale Modelling and Coreflood Simulation. Presented at the International Symposium of the Society of Core Analysts, Toronto, Canada.

Oliver, D.S., Chen, Y., 2011. Recent Progress on Reservoir History Matching: a Review. Comput Geosci 15, 185–221. doi:10.1007/s10596-010-9194-2

Oliver, D.S., Reynolds, A.C., Liu, N., 2008. Inverse Theory for Petroleum Reservoir Characterization and History Matching. Cambridge University Press.

Ott, H., Berg, S., Oedai, S., 2011. Displacement and Mass Transfer of CO_2/Brine in Sandstone. International Symposium of the Society of Core Analysts, Austin, Texas, USA, September 18–21, 2011, SCA2011-05.

Ott, H., Oedai, S., Pentland, C.H., Eide-Engdahl, K., van der Linden, A.J., Gharbi, O, Bauer, A. and Makurat, A., 2013. CO_2 Reactive Transport: Flow Regimes, Fluid Flow and Mechanical Rock Properties, International Symposium of the Society of Core Analysts, Napa Valley, California, USA, 16–19 September, 2013, SCA2013-29.

Perrin, J.-C., Benson, S., 2010. An Experimental Study on the Influence of Subcore Scale Heterogeneities on CO_2 Distribution in Reservoir Rocks, Transport in Porous Media, 82, 93–109. doi:10.1007/s11242-009-9426-x

Por, G.J., Boerrigter, P., Maas, J.G., A., de, 1989. A Fractured Reservoir Simulator Capable of Modeling Block-Block Interaction. Society of Petroleum Engineers. doi:10.2118/19807-MS

Rwechungura, R., Dadashpour, M., Kleppe, J., 2011. Advanced History Matching Techniques Reviewed. Presented at the SPE Middle East Oil and Gas Show and Conference, 25–28 September, Manama, Bahrain, Society of Petroleum Engineers. doi:10.2118/142497-MS

Wang, J., Buckley, J.S., 2006. Automatic History Matching Using Differential Evolution Algorithm. Presented at the International Symposium of the Society of Core Analysts, Trondheim, Norway.

Table 1. Summary of the observed data used in the assisted history matching process. The early time observations coincide with the breakthrough time (pressure difference data) or approximately with a levelling off in the water production data. All observed data points are assigned equal weighting.

	decane-brine		**CO_2-brine**	
	Early Time	Late Time	Early Time	Late Time
time (hours)	7.63	21.04	3.82	10.57
Water Produced (mL)	48.24 (± 1)	48.48 (± 1)	39.09 (± 1)	39.64 (± 1)
time (hours)	2.60	21.04	0.80	6.62
Pressure Difference (bar)	0.126 (± 5%)	0.105 (± 5%)	0.076 (± 5%)	0.061 (± 5%)

Table 2. Summary of the parameterized functions of relative permeability investigated in this study.

Model	**Reference**	**Primary Drainage Equation krw‡**	**Primary Drainage Equation krnw‡**	**Variable Parameters***
Corey	Brooks and Corey, 1964	$k_{rw} = \left(\frac{S_w - S_{wc}}{1 - S_{wc}}\right)^{n_w}$	$k_{rnw} = k_{rnw}^{w}\left(\frac{1 - S_w}{1 - S_{wc}}\right)^{n_{nw}}$	k_{rnw}^{w}, n_{nw}, n_{w}
Mod. Corey	Masalmeh et al., 2007	$k_{rw} = \left(\frac{S_w - S_{wc}}{1 - S_{wc}}\right)^{n_w} + \frac{c_w}{1 + c_w}\left(\frac{S_w - S_{wc}}{1 - S_{wc}}\right)$	$k_{rnw} = k_{rnw}^{w}\left(\frac{1 - S_w}{1 - S_{wc}}\right)^{n_{nw}}$	k_{rnw}^{w}, c_{w}, n_{nw}, n_{w}
LET †	Lomeland et al., 2005	$k_{rw} = \frac{S_{wn}{}^{L_w^{nw}}}{S_{wn}{}^{L_w^{nw}} + E_w^{nw}(1 - S_{wn})^{T_w^{nw}}}$	$k_{rnw} = k_{rnw}^{w}\frac{(1 - S_{wn})^{L_{nw}^{w}}}{(1 - S_{wn})^{L_w^{nw}} + E_{nw}^{w}S_{wn}{}^{T_{nw}^{w}}}$	k_{rnw}^{w}, L_w^{nw}, E_w^{nw}, T_w^{nw}, L_{nw}^{w}, E_{nw}^{w}, T_{nw}^{w}

* In our analysis we used a fixed S_{wc} of 0.2 in all cases. It should be noted that the shape of the relative permeability curves below a water saturation of 0.6 does not affect the history match as saturations in this range were not reached in the experiments (cf. Figures 1 and 2).

† The normalized water saturation (S_{wn}) in the LET model is given by: $S_{wn} = \frac{S_w - S_{wc}}{1 - S_{wc} - S_{nwr}}$, which for primary drainage can be simplified as $S_{wn} = \frac{S_w - S_{wi}}{1 - S_{wi}}$.

‡ The relative permeability equations are formulated for the primary drainage flow sequence and hence may differ slightly from those given in the original references. Differences are due to the omission of the wetting phase end point relative permeability from the wetting phase equations. Since the primary drainage flow sequence is considered this end point relative permeability is equal to unity.

Table 3. Summary of the parameter ranges used in the assisted history matching study.

Model	**Variable Parameter**	**decane-brine**			**CO_2-brine**		
		min	**base**	**max**	**min**	**base**	**max**
Corey	n_w	2.0	15.0	20.0	5.0	20.0	30.0
	n_{nw}	1.0	1.75	2.5	1.5	1.9	3.5
	k^w_{rnw}	0.5	0.7	0.9	0.3	0.6	0.9
Modified Corey	n_w	2.0	15.0	20.0	5.0	20.0	30.0
	n_{nw}	1.0	1.75	2.5	1.5	1.9	3.5
	k^w_{rnw}	0.5	0.7	0.9	0.3	0.6	0.9
	c_w	0.0	0.001	0.01	0.0	0.001	0.01
LET	k^w_{rnw}	0.5	0.7	0.9	0.5	0.7	0.9
	L^{nw}_w	10.0	15.0	30.0	10.0	15.0	30.0
	E^{nw}_w	0.1	1.0	10.0	0.1	1.0	10.0
	T^{nw}_w	0.5	1.0	2.0	0.5	1.0	2.0
	L^w_{nw}	1.5	2.0	2.5	1.5	2.0	2.5
	E^w_{nw}	0.5	1.0	2.0	0.5	1.0	2.0
	T^w_{nw}	0.5	1.0	2.0	0.5	1.0	2.0

Table 4. Summary of the root-mean-square-errors (RMSE) between measured observable points and simulated responses for the parameterizations resulting from the history matching exercise.

	decane-brine RMSE	**CO_2-brine RMSE**
Corey	1.65	1.35
Modified Corey	1.49	1.27
LET	1.34	2.65

Table 5. Summary of the best match relative permeability parameter values.

	decane-brine (LET)							**CO_2-brine (Modified Corey)**			
Parameter	k^w_{rnw}	L^{nw}_w	E^{nw}_w	T^{nw}_w	T^{nw}_w	E^w_{nw}	T^w_{nw}	k^w_{rnw}	c_w	n_w	n_{nw}
Value	0.734	12.9	4.3	1.21	2.23	0.80	1.57	0.771	1.72×10^{-4}	18.5	3.15

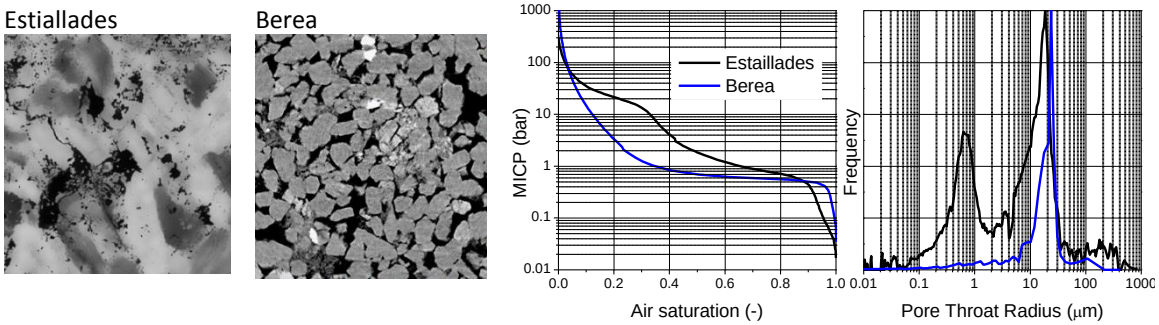

Figure 1: Left: μCT images of Estaillades limestone and Berea sandstone. Middle and right: MICP curves and normalized pore throat distribution of the same rock types.

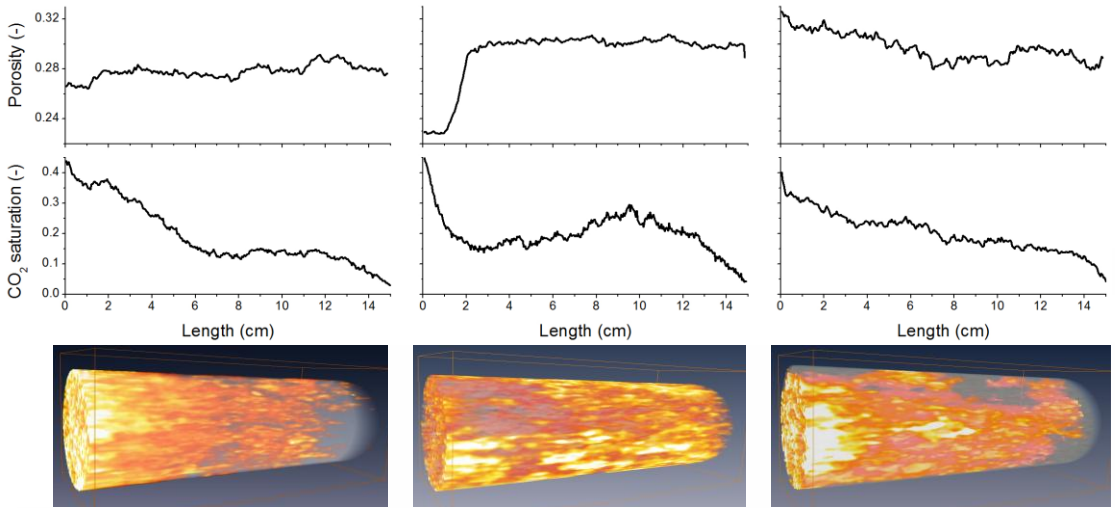

Figure 2: 1-D porosity profile (top), 1-D (middle) and 3-D (bottom) CO_2-saturation profile after primary drainage of three core floods in three different Estaillades samples. The experiment on the right is the one discussed in this paper. Note that the contrast has been chosen to highlight the heterogeneity in the saturation profile.

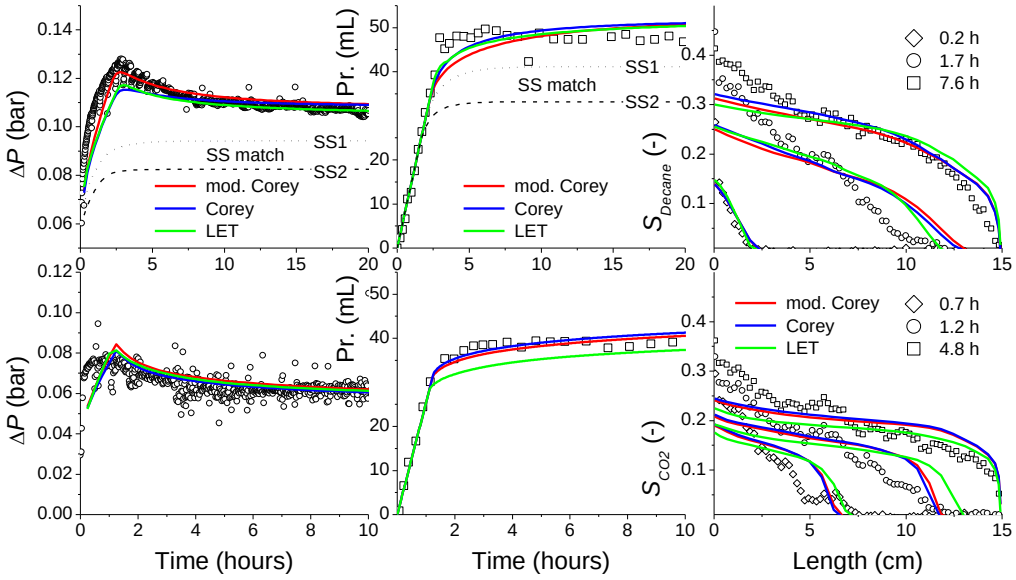

Figure 3: Simulated data from the assisted history matching study compared to the measured data for the decane-brine experiment (upper panels) and CO_2-brine experiment (lower panels).

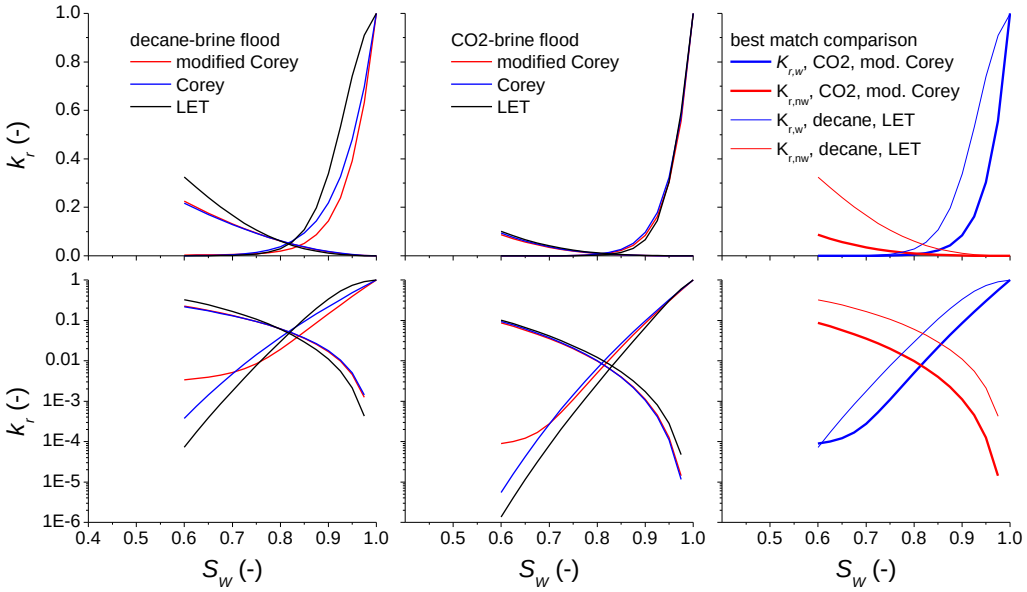

Figure 4: The best match relative permeability relationships resulting from the assisted history matching exercise. The left panels show the decane-brine relative permeabilities, the middle panels show the CO_2-brine relative permeabilities, and the right panels show a comparison of the best (lowest RMSE, Table 4).

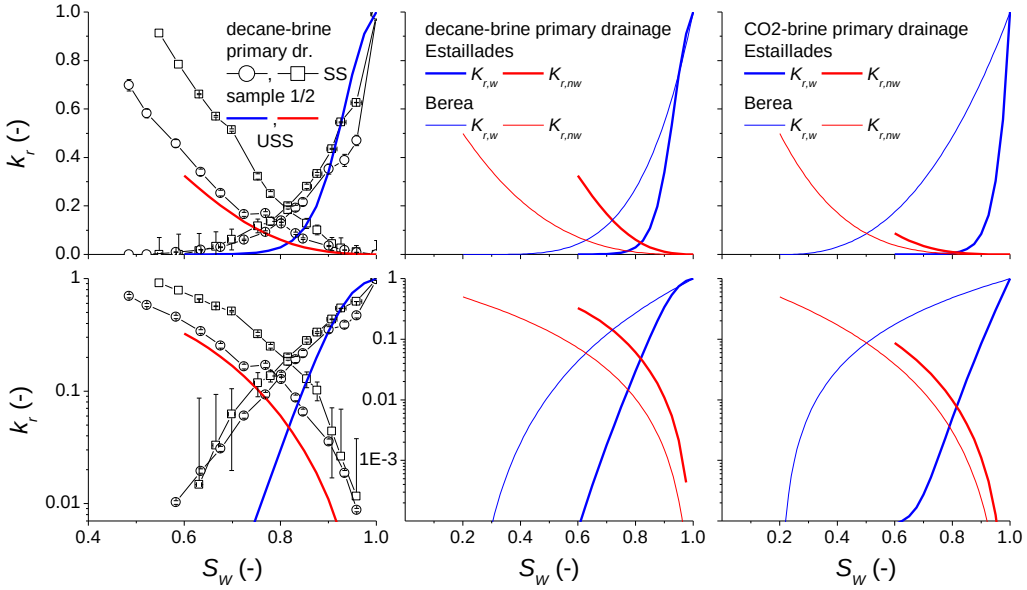

Figure 5: Left panels: comparison of results from decane-brine USS (lines) and SS (symbols—circles (SS1 in Fig. 3) and squares (SS2 in Fig. 3) represent two experiments on different samples) core floods. Middle and right panels: comparison of data obtained from Estaillades limestone and Berea sandstone for decane-brine experiments (middle) and CO_2-brine experiments (right).